

Abouelmagd Abdelsamie\*, David O. Lignell  
and Dominique Thévenin

# Comparison Between ODT and DNS for Ignition Occurrence in Turbulent Premixed Jet Combustion: Safety-Relevant Applications

DOI 10.1515/zpch-2016-0902

Received October 3, 2016; accepted June 7, 2017

**Abstract:** This work investigates the ability of the one-dimensional turbulence model (ODT) to detect, in a predictive manner, occurrence of successful ignition or misfire in a reacting gas mixture subjected to turbulence. Since ODT is computationally very efficient, this significantly aids in the analysis of safety-relevant applications. ODT delivers fast predictions, while still capturing most relevant physicochemical processes controlling ignition. However, ODT contains some empirical parameters that must be set by comparison with reliable reference data. In order to determine these parameters and check the accuracy of resulting ODT predictions, they are compared in this work with reference data from direct numerical simulation (DNS). DNS is recognized as the most accurate numerical tool to investigate ignition in turbulent flows. However, it requires very high computational times, so that it cannot be used for practical safety predictions. It is demonstrated in this article that, thanks to validation and comparison with DNS, ODT realizations can be used to predict correctly the occurrence of ignition in turbulent premixed flames while saving more than 90% of the required computational time, memory and disk space.

**Keywords:** DNS; Ignition probability; ODT; premixed flame; safety; turbulent jet.

---

\*Corresponding author: **Abouelmagd Abdelsamie**, University of Magdeburg “Otto von Guericke”, Universitätsplatz, 2, D-39106, Magdeburg, Germany, Tel.: +49-391-6712427, Fax: +49-391-6712840, E-mail: abouelmagd.abdelsamie@ovgu.de

**David O. Lignell:** Brigham Young University, 350 Clyde Building, UT-84602, Provo, USA

**Dominique Thévenin:** University of Magdeburg “Otto von Guericke”, Universitätsplatz, 2, D-39106, Magdeburg, Germany

# 1 Introduction

The physicochemical processes leading to ignition of a reactive mixture have been extensively investigated during the last few decades, demonstrating both the importance and the complexity of this issue. Most early studies of ignition phenomena from the point of view of safety analysis could only rely on experimental measurements and simplified theoretical models, like those reported in the seminal book of Lewis and von Elbe [1]. This is due to the fact that ignition is a fully coupled process involving two main aspects: (1) chemistry and (2) heat transfer, both mostly in a turbulent environment. Chemical kinetics describe the evolution of all radicals needed for the onset of ignition. A quantitative investigation taking this into account can only be realized if all relevant chemical pathways are known, if the corresponding reaction parameters have been determined accurately, and if the available computational power is sufficient to carry out corresponding simulations, involving possibly hundreds or thousands of individual reactions. Hence, the challenge associated with this issue completely depends on the composition of the mixture considered, in particular on the fuel. Second, heat exchange processes with the surroundings will be essential to determine if the ignition event will be successful and lead to a fully developed flame, or if it will fail after a short time. In order to take this aspect into account, all relevant heat exchange paths must be described accurately. A reliable quantitative study then necessitates an accurate description of the local turbulent flow conditions and of all relevant transport properties. The challenges associated with this second aspect depend on the flow conditions (laminar vs. turbulent) and on the configuration (premixed vs. non-premixed, possible interaction with surfaces, possible importance of radiative heat transfer, evaporation, etc.).

In the present work, only the ignition of premixed systems is considered, so that fuel and oxidizer are always well-mixed in advance. Due to the progress in computing power, realistic simulations accounting for the surrounding turbulent flow conditions, and thus the convective and conductive heat exchange, became possible in the early nineties. Corresponding results are found, for instance, in [2, 3] for two-dimensional (2D) flows employing a single-step chemical reaction to describe oxidation. The obtained observations have been discussed in [4, 5], demonstrating, in particular, the interest in direct numerical simulations (DNS) to investigate such configurations. Nevertheless, the probability of successful ignition could not be considered using DNS and realistic chemical kinetics at this early stage. Later works consider more realistic kinetics in 2D flows (e.g. [6]) or in 3D conditions but with simplified kinetic descriptions (one-step chemistry, for instance in [7–9]). Later DNS studies considered 3D flames with complex kinetic schemes (see e.g. [10, 11]) but did not investigate specifically ignition probability.

DNS is recognized as the most accurate tool to investigate ignition of a premixed system. However, quantifying ignition probability in connection with turbulence requires many realizations, due to the stochastic nature of turbulent coupling. Repeating in a parametric study many DNS in 3D while taking into account complex kinetics is simply impossible on current computers. Therefore, a suitable alternative is needed, possibly in connection with a few isolated DNS simulations. After checking thoroughly the scientific literature, a proper tool appears to be the one-dimensional turbulence model (ODT), which was developed first for cold flows by Kerstein [12]. This model has undergone continual improvement since then. A vector formulation of this model was introduced by Kerstein et al. [13]. Ashurst and Kerstein [14] developed a variable-density formulation, and also introduced a spatial formulation of the model in which all variables evolve along lines in space, invoking standard boundary layer assumptions. This variable-density formulation is crucial for combustion simulations. ODT has been applied to many different combustion systems. Echehki et al. [15] applied the ODT model to turbulent jet diffusion flames. Hewson and Kerstein used the model directly to study syngas flames [16], including a detailed study of flame extinction and reignition [17]. Gupta and Echehki [18] investigated autoignition in spatially-evolving jet diffusion flames. Punati et al. [19] compared ODT with DNS for a temporally-evolving jet diffusion flame. Lignell and Rappleye [20] studied extinction and reignition in spatially-evolving jet flames. Jozefik et al. [21] improved the classical ODT model to include an efficient compressible implementation and a model for capturing shock-induced turbulence. Unfortunately, all these interesting studies have considered non-premixed systems, and cannot therefore directly be used for our current objectives.

Very recently, Jozefik et al. [22] evaluated the ability of ODT to simulate a premixed flame in a counterflow configuration by comparing it with a DNS dataset. They modified the standard ODT model by adding a new term to mimic the counterflow stagnation effect. They found good agreement between their ODT results and that from DNS, especially for temperature and species fields (both mean and RMS). Punati et al. [23] performed ODT simulations of a planar, premixed hydrogen jet flame at two different Damköhler numbers, again compared with DNS results. They primarily investigated flame propagation processes, and found that standard ODT showed qualitative agreement of the overall flame evolution and temperature profiles, whereas the net fuel consumption rate was over- or under-predicted as a function of time. Based on these results, the authors stated that standard ODT cannot reproduce exactly the premixed flame for the tested conditions.

In the present work, ODT is used as a complement to DNS in order to investigate ignition probability. DNS are first performed for reference cases. After

calibrating the ODT parameters with these reference values, it is checked that ODT can indeed be used to evaluate the occurrence of ignition. Based on these findings, ODT can then be used as standalone tool to compute ignition probability for safety-relevant conditions, as will be shown in a companion publication.

Since ignition involves complex kinetic paths, it is absolutely necessary to take into account sufficiently accurate reaction schemes in the numerical analysis. Appropriate kinetic schemes will be considered in this work for propane/air mixture. To the authors' knowledge, this is the first time that ODT is used in a premixed configuration involving complex fuels to investigate autoignition. Based on this study, it must be decided if ODT is able to delineate between successful ignition and misfire when varying the peak temperature of the initial mixture.

This paper is organized as follows: the governing equations for both DNS and ODT are reviewed in Section 2; the numerical settings are explained in Section 3; the main results are discussed in Section 4, followed by a discussion of the advantages and drawbacks of ODT for this problem in Section 5, and closing with conclusions.

## 2 Governing equations

DNS and ODT involve different sets of equations and formulations, described as follows.

### 2.1 DNS

A 3D low-Mach number formulation based on the complete Navier-Stokes equations is considered in DNS [24]. The total mass conservation (continuity) equation is

$$\frac{\partial \rho}{\partial t} + \frac{\partial(\rho u_i)}{\partial x_i} = 0, \quad (1)$$

where  $\rho$  and  $u_i$  are the flow density and  $i$ -th component of the flow velocity, respectively. The reaction scheme involves a total of  $N_s$  species. The mass conservation equation for species  $k$  is

$$\frac{\partial(\rho Y_k)}{\partial t} + \frac{\partial(\rho u_i Y_k)}{\partial x_i} = -\frac{\partial(\rho V_{k,i} Y_k)}{\partial x_i} + \dot{\omega}_k, \quad \text{for } k = 1, 2, \dots, N_s. \quad (2)$$

In this equation, the mass fractions  $Y_k$ , diffusion velocities  $V_{k,i}$ , and the reaction rate  $\dot{\omega}$  should fulfill the following compatibility relations:

$$\sum_{k=1}^{N_s} Y_k = 1, \quad (3)$$

$$\sum_{k=1}^{N_s} Y_k \mathbf{V}_k = 0, \quad (4)$$

$$\sum_{k=1}^{N_s} \dot{\omega}_k = 0. \quad (5)$$

The momentum conservation equation is written as :

$$\frac{\partial(\rho u_i)}{\partial t} + \frac{\partial(\rho u_i u_j)}{\partial x_j} = -\frac{\partial p}{\partial x_i} + \frac{\partial \tau_{ji}}{\partial x_j}, \quad (6)$$

where the dynamic pressure  $p$  is computed by solving a Poisson equation (see [24] for details), and the components  $\tau_{ji}$  of the viscous tensor are defined by:

$$\tau_{ji} = -\frac{2}{3}\mu \frac{\partial u_k}{\partial x_k} \delta_{ji} + \mu \left( \frac{\partial u_j}{\partial x_i} + \frac{\partial u_i}{\partial x_j} \right). \quad (7)$$

In the low-Mach number model the energy equation can be cast as a temperature equation, as follows:

$$\rho C_p \frac{DT}{Dt} = -\sum_{k=1}^{N_s} h_k \dot{\omega}_k + \frac{\partial}{\partial x_i} \left( \lambda \frac{\partial T}{\partial x_i} \right) - \frac{\partial}{\partial x_i} \left( \rho \sum_{k=1}^{N_s} h_{s,k} Y_k V_{k,i} \right). \quad (8)$$

In Eqs. (7)–(8),  $\mu$ ,  $\delta_{ji}$ ,  $C_p$ ,  $T$ ,  $h_k$ , and  $\lambda$  are the dynamic viscosity of the mixture, Kronecker delta, specific heat at constant pressure, mixture temperature, enthalpy of species  $k$ , and heat diffusion coefficient, respectively. All details concerning the computational procedure, for instance concerning the diffusion velocity, can be found in [24].

## 2.2 ODT

In the low-Mach number DNS solver, the diffusion and advection process are considered simultaneously. On the other hand, the ODT model handles these processes in two separate, but coupled steps. The following is an explanation of ODT as reviewed

in [20]. The diffusive advancement is simulated by solving a one-dimensional form of the Navier-Stokes equation, without advection terms nor implicit pressure fluctuation treatment. Instead, the diffusive advancement is implemented using a Lagrangian finite-volume method, in which cell faces move with the mass-average velocity. In the ODT simulation, the cells expand or contract due to flow dilatation arising from heat or mass transfer processes. More details about these equations and their connection to the Navier-Stokes equation can be found in [20, 25].

The omitted advection terms are modeled with discrete mapping events of the scalar fields, which represent the turbulent advection process. These mapping processes are termed *eddy events*, and are implemented as triplet maps that rearrange the fluid domain and mimic the effect of turbulence. These triplet maps occur concurrently with the diffusion processes, and are parameterized by a size  $l$ , position  $y_0$ , and time scale  $\tau$ . The triplet map is implemented by taking all variable profiles in the eddy region, making three copies, compressing each of them spatially by a factor of three, and replacing the original profiles by the three compressed copies with the middle copy inverted spatially. The triplet map is conservative of all quantities and is defined as

$$f(y) = \begin{cases} 3(y - y_0) & \text{if } y_0 \leq y \leq y_0 + l/3, \\ 2l - 3(y - y_0) & \text{if } y_0 + l/3 \leq y \leq y_0 + 2l/3, \\ 3(y - y_0) - l & \text{if } y_0 + 2l/3 \leq y \leq y_0 + l, \\ y - y_0 & \text{otherwise.} \end{cases} \quad (9)$$

The ODT velocity profile evolves through the specification of the occurrences of eddy events. The eddy selection process is stochastic and follows the variable density formulation first introduced in [14], modified as described in [20]. In this formulation, the eddy time scale  $\tau$  for a candidate eddy ( $y_0, l$ ) is computed using (1) a measure  $E_{\text{kin}}$  of the local kinetic energy in the eddy region, and (2) the scaling:  $E_{\text{kin}} = 0.5\rho_0 l^3/\tau^2$ , where  $\rho_0$  is a density in the eddy region. The local rate (per square length) of each eddy is

$$\lambda = \frac{1}{l^2\tau}, \quad (10)$$

and the total rate of all eddies is

$$\Lambda = \iint \lambda dy_0 dl. \quad (11)$$

These can be used to define a joint PDF of eddy parameters  $y_0$  and  $l$ :

$$P(y_0, l) = \lambda(y_0, l) / \Lambda. \quad (12)$$

Eddy occurrences can be sampled from a Poisson distribution with mean rate  $\Lambda$ , with  $y_0$  and  $l$  parameters sampled from  $P(y_0, l)$ .

The eddy time scale  $\tau$ , which is used to specify the eddy acceptance probability, is computed as

$$\frac{1}{\tau} = C \sqrt{\frac{2}{\rho_0 l^3} (E_{\text{kin}} - Z E_{\text{vp}})}. \quad (13)$$

In this equation,  $\rho_0 = l^{-3} \int \rho K(y)^2 dy$  is a measure of the density in the eddy region for variable density flow, with  $K(y)$  the kernel function used in the vector formulation of ODT. ( $K(y)$  is the fluid displacement distance due to an eddy event.)  $E_{\text{vp}}$  is a viscous penalty term; it suppresses small eddies that are subject to strong viscous damping and is modeled using scaling arguments as  $E_{\text{vp}} = \bar{\rho} \bar{\nu} / l$ , where  $\bar{\rho}$  and  $\bar{\nu}$  are the average density and kinematic viscosity, respectively, in the eddy region. The parameters  $C$  and  $Z$  are adjustable model parameters. For open domains, a restriction must be imposed on the eddy selection process in order to prevent unphysically large eddy events from occurring. Suppression of large eddies is obtained using the elapsed time method, following [15, 16, 20, 25]. The corresponding criterion is

$$t > \beta \tau. \quad (14)$$

This large eddy suppression is applied in such a way that the eddies are only allowed if the elapsed time is greater than  $\beta \tau$ , where  $\beta$  is an adjustable parameter as well. Therefore, there are three significant empirical parameters in ODT that need to be adjusted:  $C$ ,  $Z$ , and  $\beta$ , though the sensitivity of ODT results to  $Z$  is normally small.

Given the eddy timescale  $\tau$ , eddies are sampled as follows. In principle, eddies of size  $l$  and position  $y_0$  could be sampled from  $P(y_0, l)$  as a Poisson process with mean rate  $\Lambda$ . This is not done in practice since  $P(y_0, l)$  evolves continuously in time, and constructing the PDF is costly. Instead,  $P(y_0, l)$  is replaced with a presumed distribution of the form  $\tilde{P}(y_0, l) = g(y_0) f(l)$  where  $g(y_0)$  is taken to be uniform on the domain, and  $f(l) = A \exp(-2\tilde{l}/l)$ , where  $\tilde{l}$  is a user-selected most-probable eddy size, and  $A$  is a normalization constant. This presumed PDF is used in conjunction with a thinning process coupled with the rejection method. In a thinning process, we can sample in time as a Poisson process with mean rate  $\alpha \Lambda$ , where  $\alpha > 1$ , and then accept eddies with probability  $P_a = \Lambda / \alpha \Lambda$ . In the rejection method, eddies are sampled from the presumed  $\tilde{P}(y_0, l)$  and accepted with probability  $P_a = P / \gamma \tilde{P}$ , where  $\gamma$  is set so that  $P_a < 1$ . Combining the two methods gives

$$P_a = \frac{\Lambda}{\alpha \Lambda} \frac{P}{\gamma \tilde{P}}. \quad (15)$$

Now, if we take  $\Delta t_s = 1/\alpha\Lambda$ , insert  $\Lambda P = \lambda = 1/\tau P$ , and absorb  $1/\gamma$  into  $\Delta t_s$  we obtain

$$P_a = \frac{\Delta t_s}{\tau_e l^2 \tilde{P}}. \quad (16)$$

It is then possible to sample eddy sizes and positions from  $\tilde{P}$  at mean rate  $\Delta t_s$ , and accept them with probability  $P_a$  given in the above equation. In practice,  $\Delta t_s$  is adjusted so that  $P_a$  is small, on the order of 0.02. This method does not affect the accuracy of the sampling approach compared to using the actual  $P(y_o, l)$ , only the efficiency. This description parallels that given in [26].

### 3 Numerical setup

A temporally-evolving planar jet configuration has been considered in this work. The interest of this specific configuration for DNS studies has been discussed in more detail in [27]. This configuration is ideal for ODT, since it is statistically 1D. In this configuration, a layer of pre-heated unburned mixture is located in the center (central jet zone) of the computational domain, whereas left and right layers (co-flow zones) contain unburned mixture at a temperature of 300 K. Initial profiles of temperature and major species are illustrated along a 1D-line following the  $y$ -direction of the domain, as shown in Figure 1a. The comparisons rely on a 3D simulation for DNS, while 1D simulations are sufficient for ODT, both evolving in time. The corresponding DNS/ODT comparison is shown schematically in Figure 1b. In this figure, contours of the instantaneous temperature field are presented as a typical output from DNS, whereas the white line represents the ODT line direction. In the 3D DNS domain, the middle slab (central jet zone) moves with jet speed  $U_j$ . The surrounding co-flow zone is quiescent. An isotropic turbulent flow field is generated prior to the DNS simulation, and is used to trigger the turbulence in the central jet zone, using a hyperbolic tangent function to filter out the turbulence in the coflow. For DNS simulations, the flow is periodic in streamwise and spanwise directions, whereas it has outflow boundary conditions in the crosswise direction. The DNS simulation is performed in a domain with dimension of  $L_x = 0.7$  cm (streamwise direction),  $L_y = 0.5$  cm (crosswise direction), and  $L_z = 0.25$  cm (spanwise direction). This domain was discretized with  $n_x = 384$ ,  $n_y = 257$ , and  $n_z = 128$  grid points. In the ODT simulations, the 1D domain has a length of  $L = 0.5$  cm, initially discretized with 256 grid cells. However, it is important to mention that the ODT code used here relies on dynamic mesh adaption

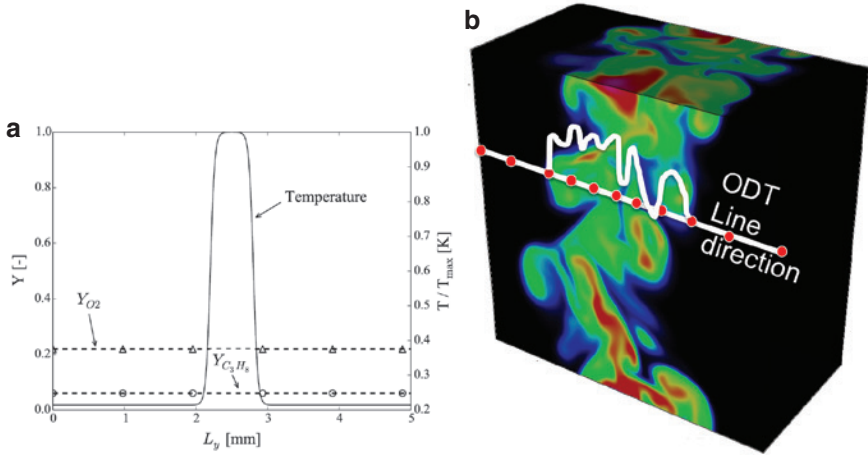


**Fig. 1:** Numerical configuration; (a) Schematic distribution of initial temperature and major species mass fractions for autoignition tests. (b) Instantaneous DNS result in the 3D domain, showing the temperature field as color contours. The white thick line along the crosswise direction, with a profile plotted along it, represents a typical 1D ODT simulation.

[25]. Therefore, the number and size of the cell is adapted automatically based on the underlying profile properties.

In this work, a stoichiometric mixture of propane/air is employed to examine the ignition occurrence in premixed, sheared turbulent flames. Again, the initial distribution of temperature and major species is illustrated in Figure 1a. The propane oxidation is described in both DNS and ODT by the GRI-mech 3.0 kinetic mechanism [28], which is implemented by relying on the open-source library CANTERA for obtaining all physicochemical and thermodynamic properties. The GRI-mech 3.0 is a well-established, optimized mechanism, built from a compilation of 325 elementary chemical reactions, involving  $N_s = 53$  chemical species. These species are  $H_2$ ,  $H$ ,  $O$ ,  $O_2$ ,  $OH$ ,  $H_2O$ ,  $HO_2$ ,  $H_2O_2$ ,  $C$ ,  $CH$ ,  $CH_2$ ,  $CH_2(S)$ ,  $CH_3$ ,  $CH_4$ ,  $CO$ ,  $CO_2$ ,  $HCO$ ,  $CH_2O$ ,  $CH_2OH$ ,  $CH_3O$ ,  $CH_3OH$ ,  $C_2H$ ,  $C_2H_2$ ,  $C_2H_3$ ,  $C_2H_4$ ,  $C_2H_5$ ,  $C_2H_6$ ,  $HCCO$ ,  $CH_2CO$ ,  $HCCOH$ ,  $N$ ,  $NH$ ,  $NH_2$ ,  $NH_3$ ,  $NNH$ ,  $NO$ ,  $NO_2$ ,  $N_2O$ ,  $HNO$ ,  $CN$ ,  $HCN$ ,  $H_2CN$ ,  $HCNN$ ,  $HCNO$ ,  $HOCN$ ,  $HNCO$ ,  $NCO$ ,  $N_2$ ,  $Ar$ ,  $C_3H_7$ ,  $C_3H_8$ ,  $CH_2CHO$ , and  $CH_3CHO$ . This mechanism has been mainly optimized to describe natural gas oxidation. The underlying optimization process did not explicitly include targets relevant to pure propane. However, many studies (e.g. [29], <http://combustion.berkeley.edu/gri-mech/version30/text30.html#propane>) compared experimental results with numerical ones based on GRI-mech 3.0 for propane flames, and showed that this mechanism agrees very well with experimental results for propane oxidation.

The DNS simulations have been conducted using a sixth-order Fortran 90 in-house solver called DINO, described in detail in [24]. The C++ parallel code developed by Lignell and co-workers [25] is used for the ODT simulations. Both codes have been running on SuperMUC, a parallel supercomputer at the Leibniz Computing Center, Munich. The parallelization in DNS relies on domain-decomposition implemented with message-passing interface (MPI). The ODT is embarrassingly parallel, with each compute core performing an independent realization.

## 4 Results

In this section four cases will be tested, as summarized in Table 1. All these cases have the same initial uniform mixture (stoichiometric  $C_3H_8/air$ ), but different initial maximum temperatures (temperature in the central jet region, see Figure 1). These cases have been selected based on preliminary studies, since autoignition will succeed in two of them ( $T_{max} = 1600$  K,  $T_{max} = 1700$  K) and fail for the other two conditions ( $T_{max} = 1400$  K,  $T_{max} = 1500$  K). In the table,  $T_{max}$ ,  $\nu_j$ , and  $Re_j$  are maximum temperature of the mixture, kinematic viscosity, and the Reynolds number in the jet region, respectively. For all cases,  $Re_j = U_j H / \nu_j$  is kept around 400, so that the turbulence intensity remains similar among the cases. In all simulations, the jet width is  $H = 0.6$  mm and the kinematic viscosity of the co-flow is  $1.49 \times 10^{-5}$  m<sup>2</sup>/s. The time in the current work is nondimensionalized using the jet flow time scale  $\tau_j = H / U_j$ . For these four cases, the Damköhler  $Da_g$  varies between 0.023 and 0.155. This Damköhler number is defined here as the ratio of jet flow time scale  $\tau_j$  to the ignition delay time  $\tau_g$ .

Even though the initial profiles for both DNS and ODT are identical, it does not mean that the turbulence-flame interaction processes are the same. To obtain the same turbulence structure and scales, the ODT parameters ( $C$ ,  $Z$ , and  $\beta$ ) first need to be tuned in an appropriate manner. After setting the underlying parameters

**Tab. 1:** Initial properties of the four cases considered to investigate autoignition with both DNS and ODT.

Case	$T_{max}$	$U_j$ (m/s)	$\nu_j$ (m <sup>2</sup> /s)	$Re_j$	$Da_g$	Autoignition occurrence
Case I	1400	130	$2.01 \times 10^{-4}$	388	0.023	Fails
Case II	1500	150	$2.25 \times 10^{-4}$	400	0.053	Fails
Case III	1600	180	$2.51 \times 10^{-4}$	430	0.095	Success
Case IV	1700	200	$2.77 \times 10^{-4}$	433	0.155	Success

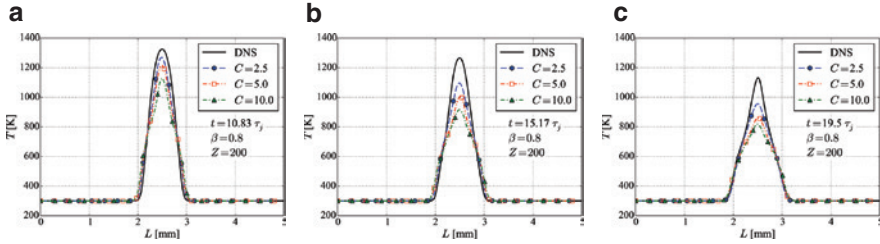


Fig. 2: Time-evolution of ensemble-averaged temperature of Case I.

using the DNS as a reference, ODT will be used as a standalone tool and compared with the DNS in order to evaluate the possibility of using ODT to generate a probability map for different parameters, opening the door for later systematic studies relevant for safety predictions.

## 4.1 ODT parameter tuning

In the next sections, the ensemble-averaged statistics in DNS are obtained by computing the mean values over the streamwise and spanwise directions. The ensemble-averaged statistics in the ODT are obtained by averaging over 544 independent realizations. This number of realizations corresponds to the number of processors used simultaneously on SuperMUC for ODT simulations (34 nodes  $\times$  16 cores). It was found that the ODT statistics are converged at this number of realization, similar to observations in [19, 30].

### 4.1.1 Eddy rate parameter $C$

The eddy rate parameter  $C$  plays a very important role in the ODT simulation, since it scales the turbulent transport. Therefore, it is roughly analogous to the coefficient of an eddy-viscosity model, with the distinction that it tunes the advancement of a temporally and spatially resolved unsteady simulation, rather than an ensemble-averaged state [25]. Figures 2–5 show the comparison between DNS and ODT for three different values of  $C$  (2.5, 5.0, 10.0), while retaining  $\beta = 0.8$  and  $Z = 200$ . This initial guess for  $\beta$  and  $Z$  is obtained based on our own experience and on the observations discussed in [19]. In all cases,  $C = 2.5$  leads to ODT temperature profiles in good qualitative agreement with DNS, but with a quantitative difference. For Case I at early simulation times, ODT with  $C = 2.5$  gives good

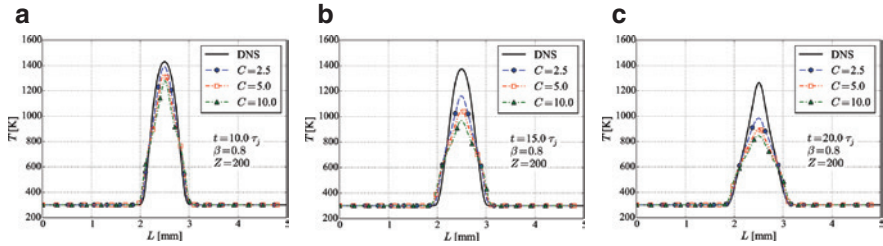


Fig. 3: Time-evolution of ensemble-averaged temperature of Case II.

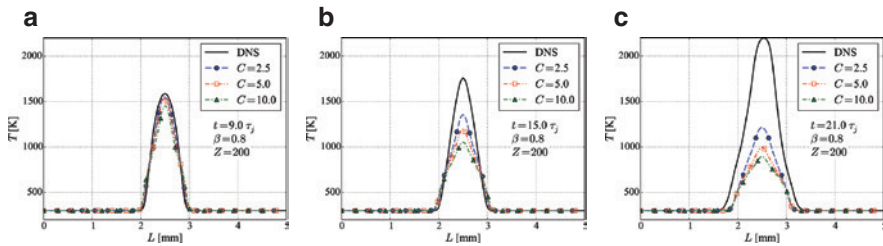


Fig. 4: Time-evolution of ensemble-averaged temperature of Case III.

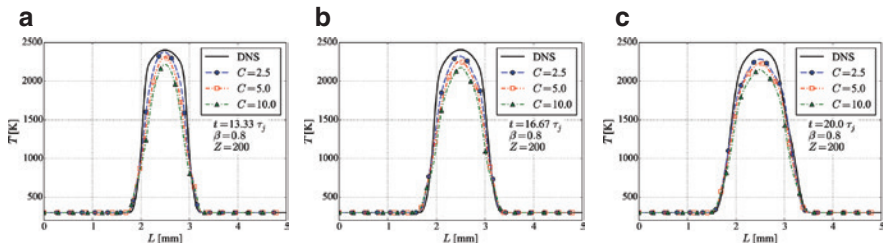


Fig. 5: Time-evolution of ensemble-averaged temperature of Case IV.

agreement with DNS as seen from Figure 2a; but it increasingly deviates with time (Figure 2b and c). A similar behavior is observed for Case II, but with a larger deviation, as seen in Figure 3a–c. However, it must be kept in mind that the only objective of this paper is to predict successful ignition or misfire, not the exact temperature profile.

Keeping this point in mind, Figure 4 shows that ODT with these same parameters unfortunately does not predict correctly autoignition for Case III. Nevertheless, it is observed that decreasing the value of  $C$  (within the chosen range: 2.5 – 10) improves the agreement between ODT and DNS.

On the other hand, decreasing  $C$  to 2.5 is sufficient in Case IV to correctly predict successful ignition. The question remains, why ODT fails in Case III but succeeds in Case IV? This is generally due to the ODT overpredicting the mixing rate, resulting in lower temperatures in all cases. These lower temperatures suppress the ignition. As the initial temperature increases with increasing case number, ignition is strengthened and is able to overcome the unfavorable mixing. However, for the given set of parameters, this does not happen until Case IV. This is largely due to the value of the  $\beta$  parameter, which controls the large eddies and strongly affects the overall mixing rate. The effect of  $\beta$  is considered in the following section. In any case, it is clear that  $C=2.5$  is the best choice among the three values investigated for the given  $Z$  and  $\beta$  chosen. This value of  $C$  is used below, and  $\beta$  and  $Z$  further considered.

#### 4.1.2 Large-eddy suppression parameter $\beta$

In this work a large-eddy suppression mechanism is required to prevent unphysically large eddies from occurring in open domains, as discussed before. These large eddies can have a considerable effect on the overall turbulent entrainment and mixing rates. The impact of  $\beta$  on the temperature profile is examined by choosing values of  $\beta = 0.8, 1.0, 1.2, 1.5$ , while keeping  $C = 2.5$  and  $Z = 200$ . The results are illustrated in Figures 6–9. It is observed that increasing  $\beta$  reduces the mixing rate by suppressing large eddies, and gives a better agreement with DNS temperature profiles. Looking closer at Case I, it is found that at early times (Figure 6a and b) ODT with  $\beta = 1.5$  shows best comparison to DNS. Later (Figure 6c) DNS profiles are found between curves of  $\beta = 1.5$  and  $\beta = 1.2$ . In Case II, ODT with  $\beta = 1.5$  is always the best choice (Figure 7); still, ODT with  $\beta = 1.2$  is close to the DNS results.

As discussed in the previous section, Case III is the most critical one, since choosing wrong parameters for ODT will lead to a wrong prediction concerning

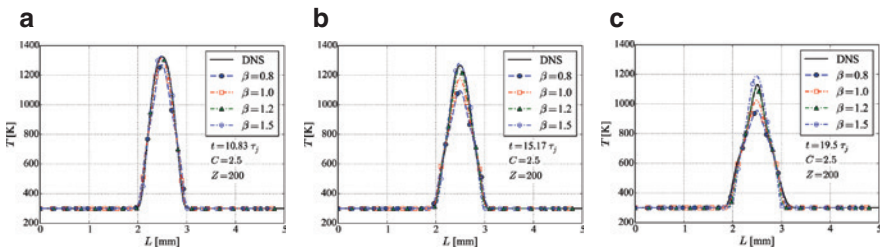


Fig. 6: Time-evolution of ensemble-averaged temperature of Case I.

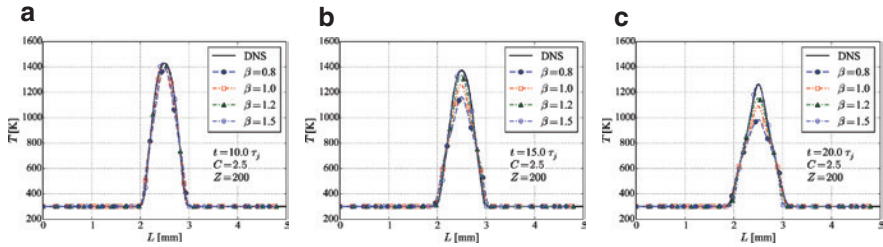


Fig. 7: Time-evolution of ensemble-averaged temperature of Case II.

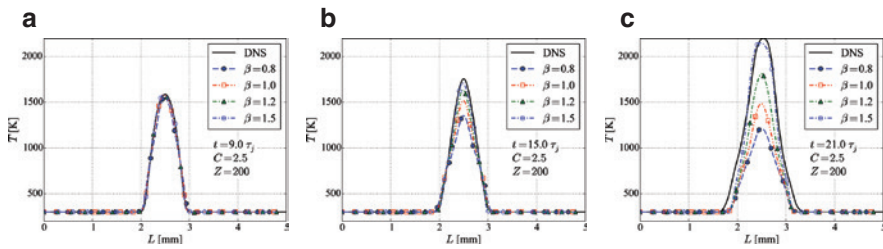


Fig. 8: Time-evolution of ensemble-averaged temperature of Case III.

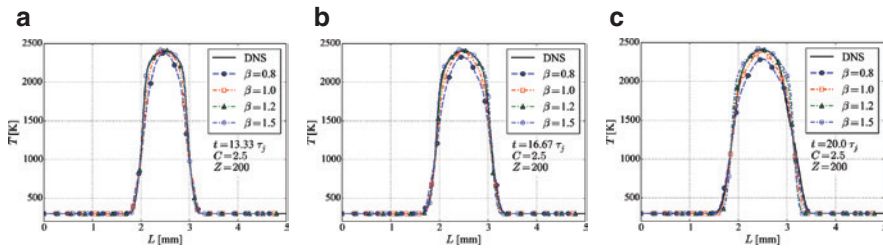


Fig. 9: Time-evolution of ensemble-averaged temperature of Case IV.

ignition success. Looking at Figure 8, it is found that ODT with  $\beta = 1.2$  and  $1.5$  both predict autoignition correctly. However, ODT with  $\beta = 1.2$  underestimates the temperature profile at later times (Figure 8c). It is also seen that ODT with  $\beta = 0.8$  and  $1.0$  underpredicts the temperature profile and leads to the wrong prediction.

As previously noted, Case IV has a high temperature and its ignition propensity and temperature profiles are less sensitive to the degree of mixing. Therefore, changing  $\beta = 1.0$  to  $1.2$  and  $1.5$  does not change much the observations in this case. We note here that there is a positive feedback between temperature and mixing as relates to ignition. That is, higher temperatures favor ignition and higher temperatures

increase viscosity and decrease density, which decreases the local Reynolds number, hence decreases local mixing rates, which further favors ignition.

In summary, choosing a value of  $\beta$  between 1.2 and 1.5 while keeping  $C=2.5$  leads to an excellent agreement between ODT and DNS, leading to correct predictions of ignition occurrence or failure for the tested conditions.

### 4.1.3 Viscous penalty parameter $Z$

The viscous penalty parameter  $Z$  is used to suppress small eddies. Usually,  $Z$  has a small impact compared to the other two parameters ( $C$  and  $\beta$ ). This is confirmed for Cases I, II and IV, where changing  $Z$  from 10 to 200 (while keeping  $C=2.5$  and  $\beta=1.5$ ) does not change in any noticeable way the temperature profiles or the occurrence of ignition. However, a slight impact of  $Z$  is observed in Case III, where ODT with  $Z=200$  shows better agreement compared to that generated by ODT with  $Z=10$  as seen in Figure 10. Hence,  $Z=200$  will be used for all further simulations.

## 4.2 ODT vs. DNS

After completing the adjustment of all ODT parameters, it is now time to have a deeper look at the ODT simulations, and see how many details can be obtained from ODT.

### 4.2.1 ODT realization with the full DNS domain

Figures 11–14 show instantaneous profiles of the temperature field in the DNS and ODT domains. These figures demonstrate the similarity between the outputs of DNS and ODT. In order to facilitate comparison, a line along the crosswise direc-

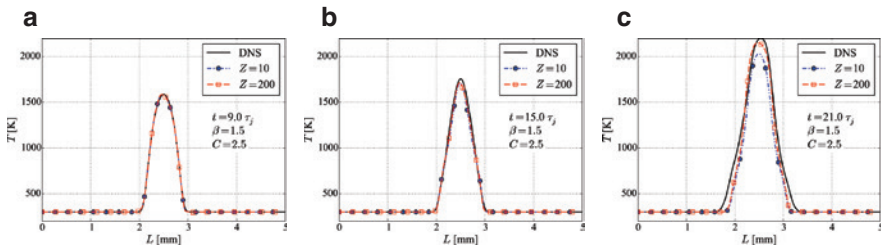
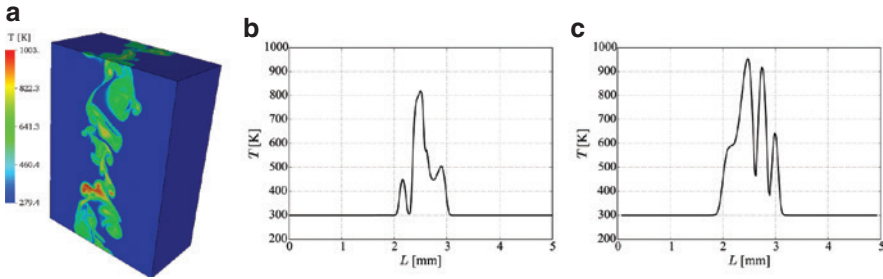
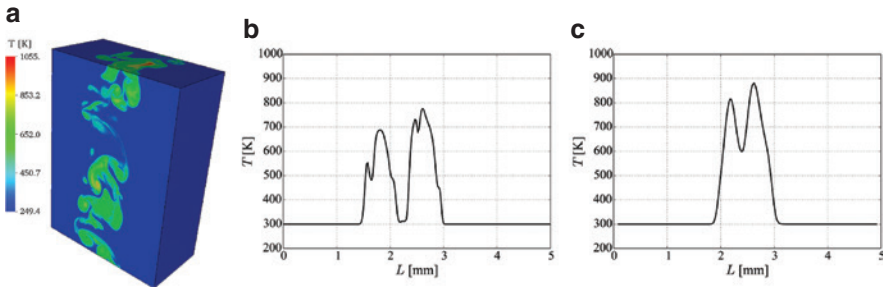


Fig. 10: Time-evolution of ensemble-averaged temperature of Case III.



**Fig. 11:** Instantaneous temperature profile at  $t = 32.6\tau_j$  for Case I: (a) Contours of DNS, (b) line taken along the crosswise direction of DNS domain, (c) an ODT realization selected randomly.



**Fig. 12:** Instantaneous temperature profile at  $t = 37.5\tau_j$  for Case II: (a) Contours of DNS, (b) line taken along the crosswise direction of DNS domain, (c) an ODT realization selected randomly.

tion of the DNS domain is taken (Figures 11b, 12b, 13b and 14b) and is qualitatively compared to a single ODT realization (Figures 11c, 12c, 13c and 14c) using the parameters,  $C = 2.5$ ,  $\beta = 1.5$ , and  $Z = 200$ . These comparisons demonstrate the qualitative ability of ODT to capture the evolution of turbulent eddies and turbulent mixing for all cases. However, it is not sufficient to judge the ability of ODT from such instantaneous figures and isolated, random realizations. Therefore, scatter plots and conditional mean have been generated to support further discussions.

#### 4.2.2 Scatter plot and conditional mean of heat release

This section discusses the ability of ODT to reproduce the heat release and its conditional mean as function of temperature, since heat release and temperature are the essential parameters in safety-relevant applications. This analysis is done by comparing scatter plots of heat release and temperature for the DNS and ODT. The ODT

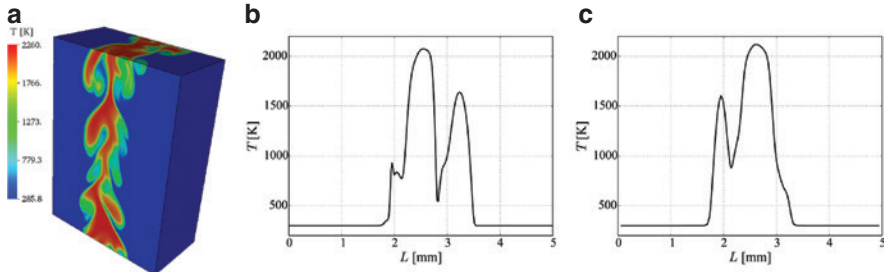


**Fig. 13:** Instantaneous temperature profile at  $t = 27.27\tau_j$  for Case III: (a) Contours of DNS, (b) line taken along the crosswise direction of DNS domain, (c) an ODT realization selected randomly.

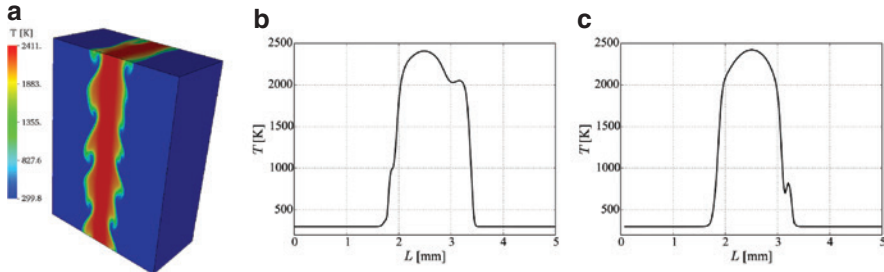


**Fig. 14:** Instantaneous temperature profile at  $t = 20.69\tau_j$  for Case IV: (a) Contours of DNS, (b) line taken along the crosswise direction of DNS domain, (c) an ODT realization selected randomly.

results are obtained by keeping  $C=2.5$ ,  $\beta=1.5$ , and  $Z=200$  for all cases, except for Case IV, for which the influence of  $\beta$  will be discussed further. Figures 15–18 are represented with three columns. The left and middle columns of these figures show the scatter plot of the heat release produced by DNS and ODT, respectively; the conditional mean of heat release is overlaid as a solid line. The conditional means of heat release obtained by DNS and ODT are compared in the last column of these figures.

For Case I (Figure 15), at early times ODT somewhat underpredicts the heat release (Figures 15a–c); and the dispersion of the initial distribution is too small. This can be also seen directly from  $\langle \text{HR} | T \rangle$  in Figure 15c, where ODT shows a slight underestimation of heat release at high temperatures. With increasing time, the structure of heat release is represented by ODT with increasing accuracy as observed both in scatter plots and for  $\langle \text{HR} | T \rangle$ . At later times,  $t = 15.2\tau_j$  and  $t = 19.5\tau_j$ , ODT reproduces the heat release scatter plot of DNS with a very good agreement.

Case II shows a slightly different behavior, as is seen in Figure 16. At early times (Figures 16a–f) the dispersion of ODT is low and does not reproduce

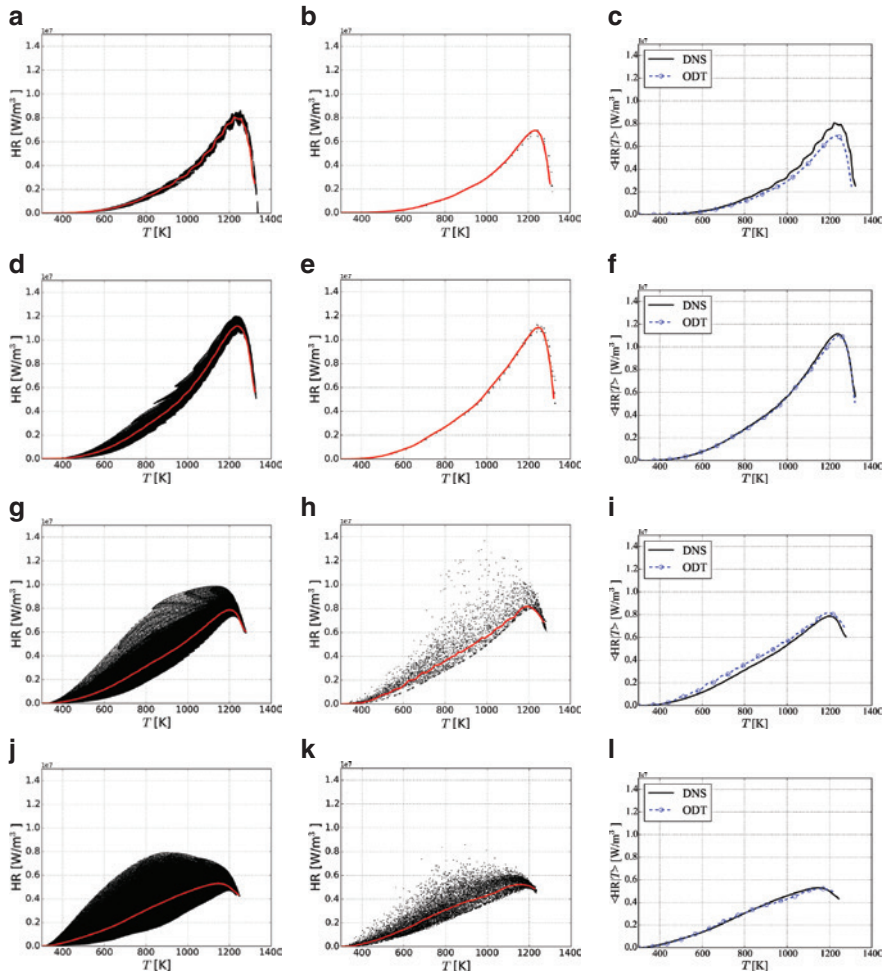


**Fig. 15:** Time-evolution of scatter plots and conditional means of heat release vs. temperature for Case I. Left column represents the DNS. Middle column represents ODT. Last column represents conditional mean of heat release in DNS and ODT. Time from top to bottom:  $t = 6.5\tau_p$ ,  $10.8\tau_p$ ,  $15.2\tau_p$ , and  $19.5\tau_p$ .

correctly the behavior of the reacting system at high temperatures ( $T > 1000$  K); this may be due to a delay of the onset of eddies in the ODT model. Given that the DNS and ODT use the same chemical mechanisms, the decreased heat release of the ODT at early times is indicative of over-prediction of diffusive transport processes (arising from eddy events) in the ODT. However, ODT later starts to agree very well with the DNS and nearly identical structures are observed at the later

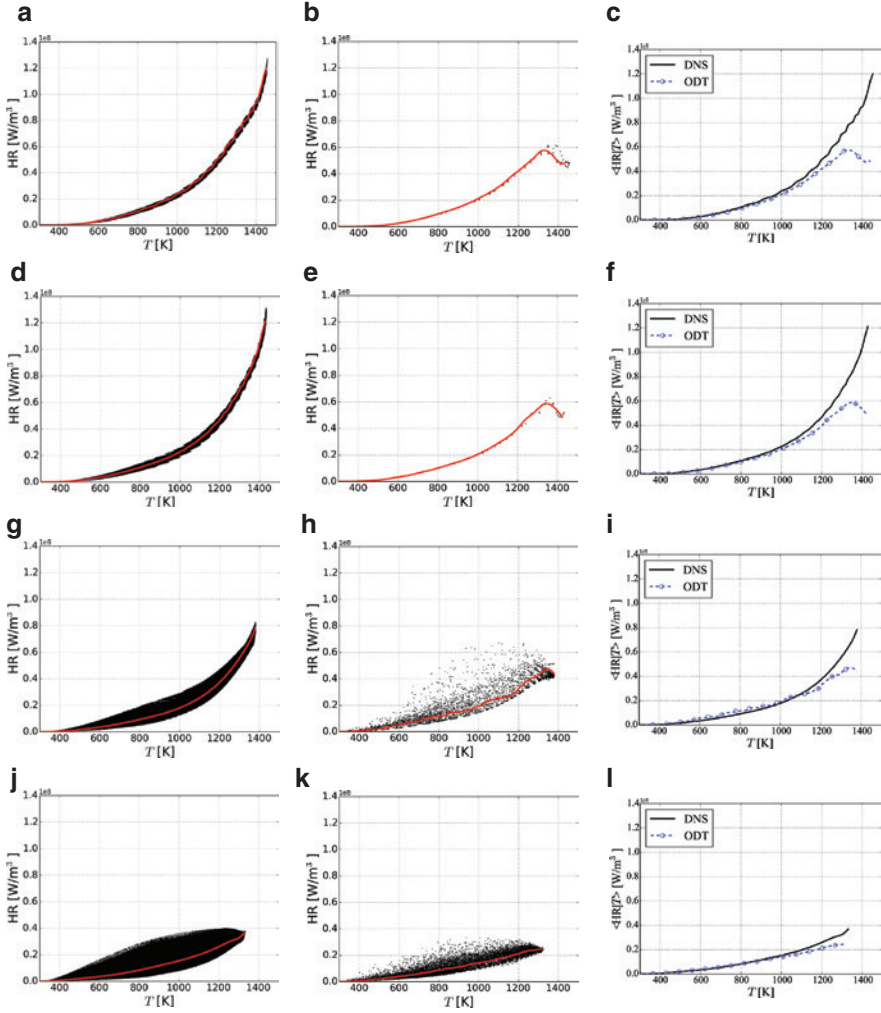


**Fig. 16:** Time-evolution of scatter plots and conditional means of heat release vs. temperature for Case II. Left column represents the DNS. Middle column represents ODT. Last column represents conditional mean of heat release in DNS and ODT. Time from top to bottom:  $t = 7.5\tau_p$ ,  $10.0\tau_p$ ,  $15.0\tau_p$ , and  $20.0\tau_p$ .

times (Figures 16j and k), apart from small differences in the conditional mean (Figure 16l) above  $T > 1000$  K.

Figure 17 demonstrates that Case III is very well reproduced by ODT; the first and middle columns show good agreement at all times. The only small deviation is observed for the conditional mean at an intermediate time  $t = 15.0\tau_p$  (Figure 17i).

Later on, at  $t \geq 21.0\tau_r$ , ODT reproduces exactly the conditional mean of heat release obtained from DNS.

Regarding finally Case IV, it was previously discussed that changing  $\beta$  from 1.0 to 1.5 did not impact noticeably the temperature (see again Figure 9).

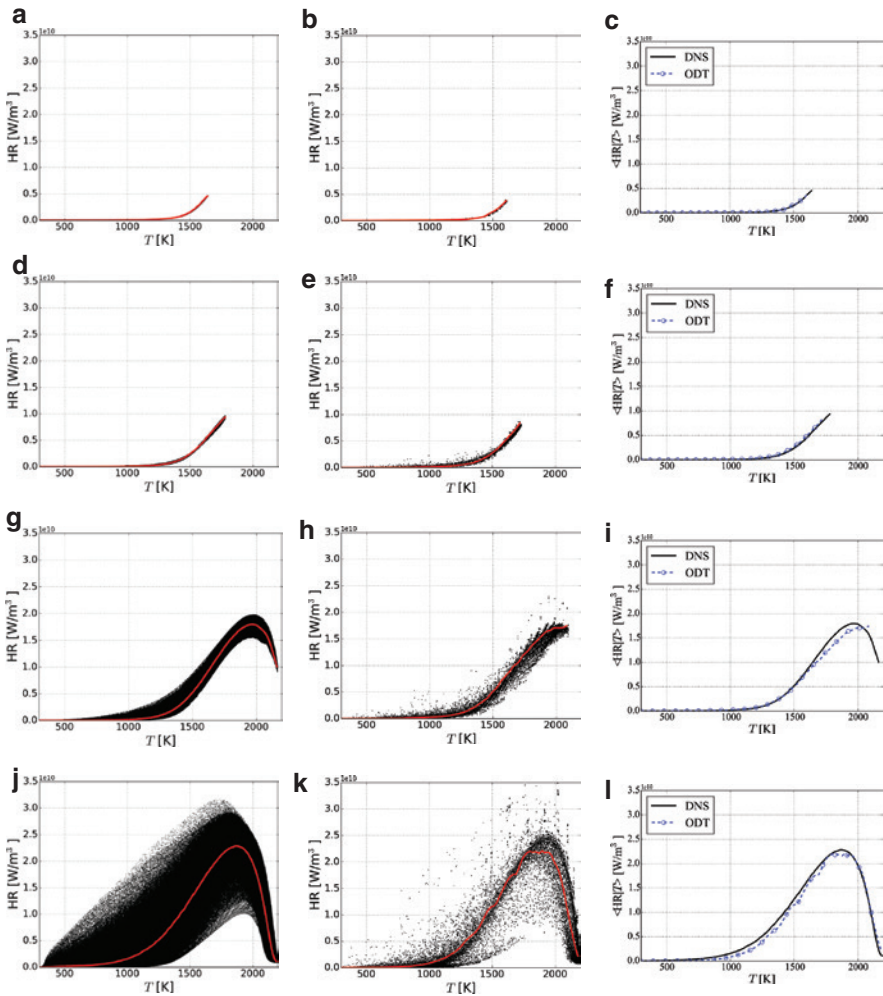


**Fig. 17:** Time-evolution of scatter plots and conditional means of heat release vs. temperature for Case III. Left column represents the DNS. Middle column represents ODT. Last column represents conditional mean of heat release in DNS and ODT. Time from top to bottom:  $t = 9.0\tau_r$ ,  $12.0\tau_r$ ,  $15.0\tau_r$ , and  $21.0\tau_r$ .

This case was first tested with  $\beta=1.5$ , but this resulted in very low dispersion compared to the DNS results. Changing the value of  $\beta$  to 1.2, the scatter plots are in much better agreement with the DNS as seen in Figures 18. The conditional means (Figure 18c, f, i and l) demonstrate that ODT results agree very well with those obtained by DNS.

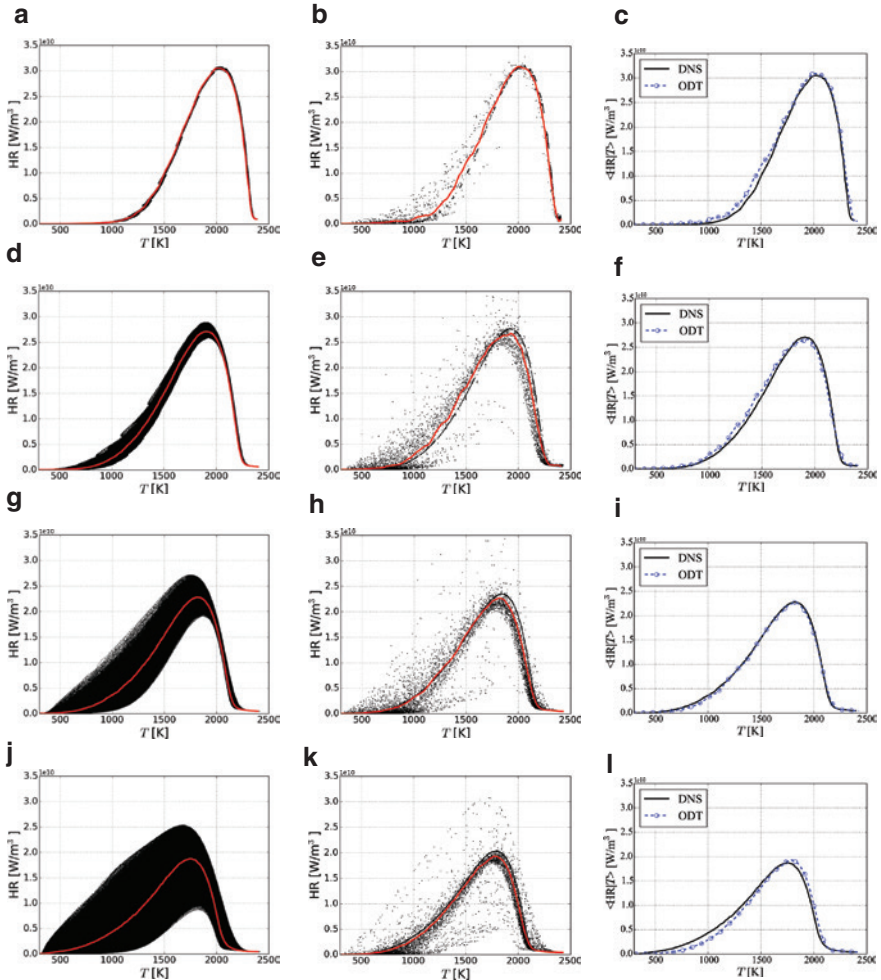


**Fig. 18:** Time-evolution of scatter plots and conditional means of heat release vs. temperature for Case IV. Left column represents the DNS. Middle column represents ODT. Last column represents conditional mean of heat release in DNS and ODT. Time from top to bottom:  $t = 10.0\tau_p$ ,  $13.3\tau_p$ ,  $16.7\tau_p$ , and  $20.0\tau_p$ .

As a conclusion of this section, it is observed that ODT is able to reproduce with good accuracy the heat release and temperature profiles for four different reference cases computed by DNS. Considering both temperature and heat release, the optimal ODT parameters for this problem are found to be  $C=2.5$ ,  $\beta=1.2-1.5$ , and  $Z=200$ . Using these parameters, ODT is able to properly distinguish between successful or failed ignition.

#### 4.2.3 Conditional means of the intermediate species OH

The radical OH is an essential intermediate for most combustion processes. OH can be considered as an indicator for chemical activity in premixed combustion [31]. Additionally, it is easily measurable, and is thus often compared with experimental data. In this section, the ability of ODT to reproduce the behavior of the OH mass fraction is examined. This is done by comparing the conditional mean

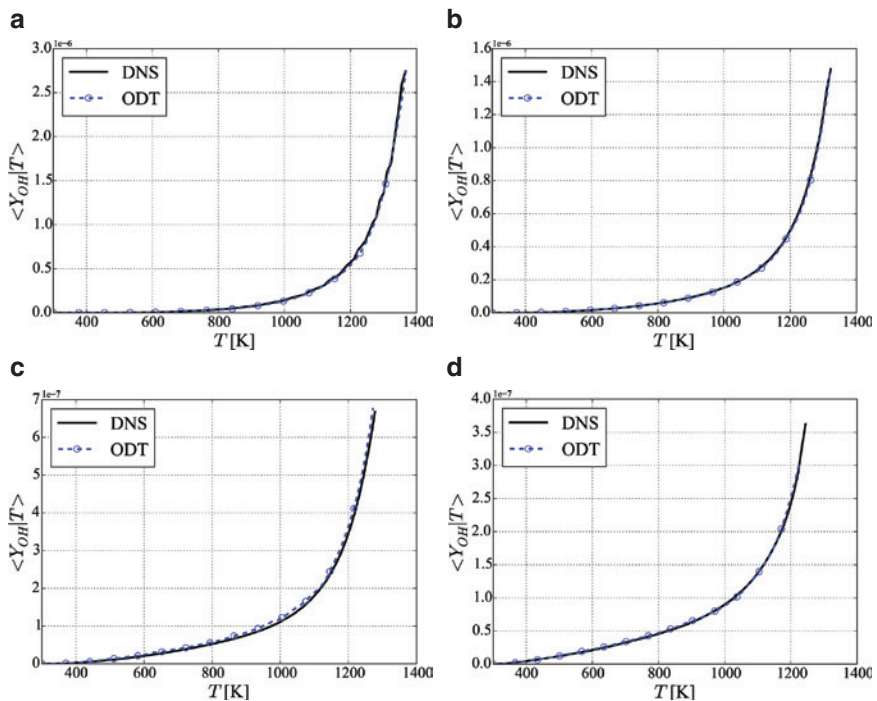


**Fig. 19:** Time-evolution of the conditional mean of  $Y_{OH}$  vs. temperature for Case I: comparing DNS with ODT. Time of subfigures a–d:  $t = 6.5\tau_p$ ,  $10.8\tau_p$ ,  $15.2\tau_p$ , and  $19.5\tau_p$ .

of the mass fraction of OH  $\langle Y_{\text{OH}} | T \rangle$  obtained by ODT or DNS for each case, at the same time  $s$  shown in the previous section. Figures 19–22 compare the profiles of  $\langle Y_{\text{OH}} | T \rangle$  obtained by DNS (solid lines) with those predicted by ODT (dashed lines with circles) for Cases I – IV, respectively. Cases I, III and IV show excellent quantitative agreement at all times. OH is sensitive to temperature and this agreement is consistent with the good temperature agreement previously shown. For Case II, good qualitative agreement is observed, but ODT systematically underpredicts the OH mass fraction at high temperature, above  $T > 1000$  K. This coincides with the observations discussed together with Figures 16c,f,i and l: the intensity of the reaction is too low at high temperatures.

It would probably be possible to obtain an even better agreement concerning these profiles by tuning more precisely the ODT model parameters. However, considering that the retained values already lead to a correct prediction of successful ignition or misfire – the central issue of this work – this point is left for further studies.

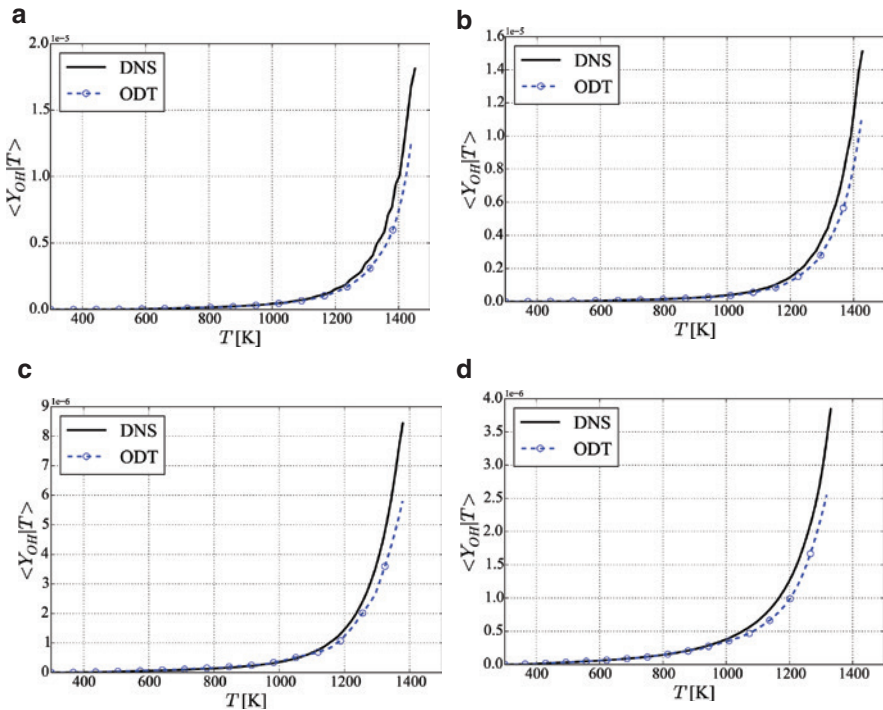


**Fig. 20:** Time-evolution of the conditional mean of  $Y_{\text{OH}}$  vs. temperature for Case II: comparing DNS with ODT. Time of subfigures a–d:  $t = 7.5\tau_r$ ,  $10.0\tau_r$ ,  $15.0\tau_r$ , and  $20.0\tau_r$ .

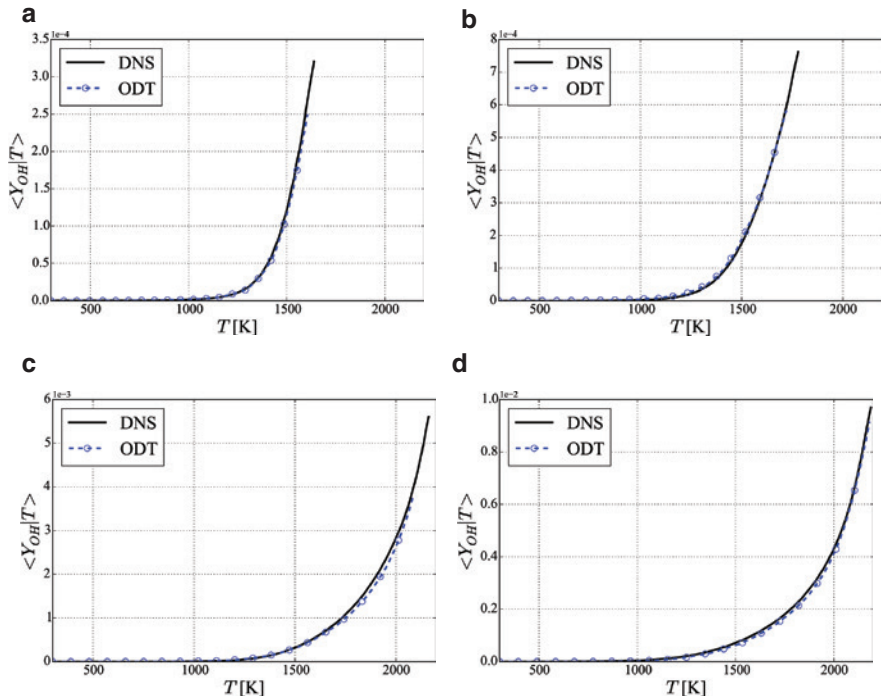


**Fig. 21:** Time-evolution of the conditional mean of  $Y_{OH}$  vs. temperature for Case III: comparing DNS with ODT. Time of subfigures a–d:  $t = 9.0\tau_p$ ,  $12.0\tau_p$ ,  $15.0\tau_p$ , and  $21.0\tau_p$ .

## 5 Advantages and drawbacks of ODT

After adjusting the free parameters  $C$ ,  $Z$ , and  $\beta$ , ODT becomes an extremely fast computational approach. The longest DNS simulation in this work consumed 73728 CPU-hours on SuperMUC; for comparison, the longest ODT simulation required 1500 CPU-hours on the same machine, but for 544 realizations. One single ODT computation takes only a few minutes. The same observation applies for the required disk space. DNS always stores 3D data, whereas ODT saves 1D profiles. While the largest DNS simulation produced roughly 500 GB of data, 500 realizations of ODT required only 5 GB. Replacing completely DNS by ODT for the current conditions and Reynolds numbers would save 97.9% of computational time and 99% of disk space. Even when considering very complex kinetic mechanisms, ODT could still be employed on a standard PC, without any need for a dedicated supercomputing system. This would make systematic safety-relevant

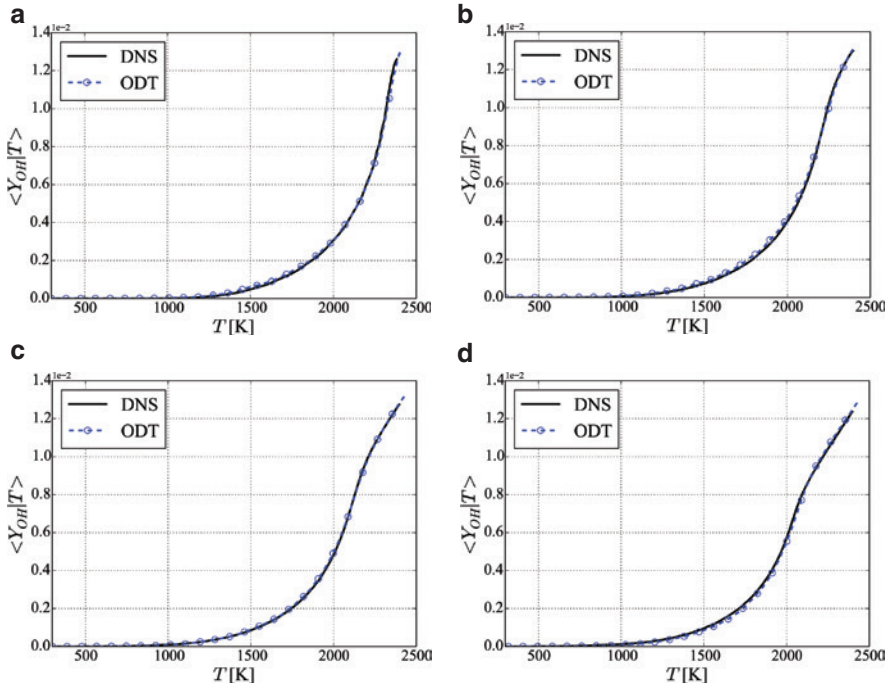


**Fig. 22:** Time-evolution of the conditional mean of  $Y_{OH}$  vs. temperature for Case IV: comparing DNS with ODT. Time of subfigures a–d:  $t = 10.0\tau_p$ ,  $13.3\tau_p$ ,  $16.7\tau_p$ , and  $20.0\tau_p$ .

studies possible. However, it is important to keep in mind that this comparison is case-dependent, and will thus vary as a function of Reynolds number and test conditions [30].

Overall, ODT appears to be an excellent tool to predict ignition probability for safety applications. In a few hours of computing time, a parametric study is possible with ODT, after tuning the model parameters by comparisons with DNS. This is a drawback of ODT; reference cases are needed (experiment or DNS) in order to fit the three free parameters for the specific configuration considered in the study.

Besides the computational cost advantage of ODT, and the free parameter disadvantage, ODT is limited to simple configurations that can be represented by standard boundary layer assumptions. This is not a significant restriction when comparing to DNS, since DNS are nearly always performed for simple, canonical flows. For evaluation of ignition phenomena where the primary consideration is the interplay between the chemistry and the turbulence, DNS and ODT appear to be sufficient. But ODT is not directly applicable to configurations with complex

geometry. Large-eddy simulations that use ODT (or LEM) as a subgrid model, and their variants, somewhat relax this constraint.

## 6 Conclusion

It has been shown in this work that ODT is able to predict success or failure of autoignition for a premixed flame in a turbulent shear flow. A temporally-evolving planar jet configuration was used for that purpose, comparing in a systematic manner ODT results with DNS observations. These comparisons show that ODT can predict both qualitatively and quantitatively temperature, heat release, and intermediate species (OH mass fraction) for a variety of initial conditions involving different temperatures and jet velocities. After fitting the three free parameters of the model, ODT is able to predict correctly the occurrence – or not – of autoignition with extremely short computational times and negligible disk-space requirements (compared to DNS), opening the door for generating ignition probability maps for safety-relevant applications. Compared to a systematic DNS study, ODT saves more than 90% of computational resources. Of course, the validity of these statements must be checked in future projects for a variety of mixture compositions, for different fuels, and at higher Reynolds numbers.

**Acknowledgements:** The financial support of the DFG (Deutsche Forschungsgemeinschaft) for Abouelmagd Abdelsamie within the project FOR1447 “Physico-chemical-based models for the prediction of safety-relevant ignition processes” is gratefully acknowledged. The computer resources provided by the Gauss Center for Supercomputing/Leibniz Supercomputing Center Munich under grant pro84qo have been essential to obtain the DNS and ODT results presented in this work. Very interesting discussions with Alan Kerstein are gratefully acknowledged.

## References

1. B. Lewis, G. von Elbe, *Combustion, Flames and Explosions of Gases*. Academic Press Inc, Orlando, Florida (1987), P. 32887, 3rd edition.
2. T. Hasegawa, A. Arai, S. Kadowaki, S. Yamaguchi, *Combust. Sci. Tech.* **84** (1992) 1.
3. M. Baum, T. Poinso, *Combust. Sci. Tech.* **106** (1995) 19.
4. T. Poinso, S. Candel, A. Trouvé, *Prog. Energy Combust. Sci.* **21** (1996) 531.
5. D. Veynante T. Poinso, *Theoretical and Numerical Combustion*. R. T. Edwards, Inc., Philadelphia, USA (2005), 2nd edition.

6. C. F. Kaminski, J. Hult, M. Aldén, S. Lindenmaier, A. Dreizler, M. Baum, U. Maas, *Proc. Combust. Inst.* **28** (2000) 339.
7. J. Hult, S. Gashi, N. Chakraborty, M. Klein, K. Jenkins, R. Cant, C. Kaminski, *Proc. Combust. Inst.* **31** (2007) 1319.
8. M. Klein, N. Chakraborty, R. S. Cant, *Flow Turb. Comb.* **81** (2008) 583.
9. N. Chakraborty, E. Mastorakos, S. Cant, *Combust. Sci. Tech.* **179** (2007) 293.
10. R. Sankaran, E. R. Hawkes, J. H. Chen, C. K. Law, T. Lu, *Proc. Combust. Inst.* **31** (2007) 1291.
11. A. J. Aspden, M. S. Day, J. B. Bell, *Combust. Flame* **166** (2016) 266.
12. A. R. Kerstein, *J. Fluids Mech.* **392** (1999) 277.
13. A. R. Kerstein, W. T. Ashurst, S. Wunsch, V. Nilse, *J. Fluid Mech.* **447** (2001) 85.
14. W. T. Ashurst, A. R. Kerstein, *Phys. Fluids* **17** (2005) 025107–1
15. T. Echekki, A. R. Kerstein, T. D. Dreeben, J.-Y. Chen, *Combust. Flame* **125** (2001) 1083.
16. J. C. Hewson, A. R. Kerstein, *Combust. Theor. Model* **5** (2001) 669.
17. J. C. Hewson, A. R. Kerstein, *Combust. Sci. Tech.* **174** (2002) 35.
18. K. G. Gupta, T. Echekki, *Combust. Flame* **158** (2011) 327.
19. N. Punati, J. C. Sutherland, E. R. Hawkes, A. R. Kerstein, J. H. Chen, *Proc. Combust. Inst.* **33** (2011) 1515.
20. D. O. Lignell, D. Rappleye, *Combust. Flame* **159** (2012) 2930.
21. Z. Jozefik, A. R. Kerstein, H. Schmidt, *Combust. Flame* **164** (2016) 53.
22. Z. Jozefik, A. R. Kerstein, H. Schmidt, S. Lyra, H. Kolla, J. H. Chen, *Combust. Flame* **162** (2015) 2999.
23. N. Punati, H. Wang, E. R. Hawkes, J. C. Sutherland, *Flow Turbulence Combust.* **97** (2016) 913.
24. A. Abdelsamie, G. Fru, T. Oster, F. Dietzsch, G. Janiga, D. Thévenin, *Comput. Fluids* **131** (2016) 123.
25. D. O. Lignell, A. R. Kerstein, E. I. Monson, *Ther. Comput. Fluid Dyn.* **27** (2013) 273.
26. G. Sun, J. C. Hewson, D. O. Lignell, *Int. J. Multiph. Flow* **89** (2017) 108.
27. A. Abdelsamie, D. Thévenin, *Proc. Combust. Inst.* **36** (2017) 2493.
28. G. P. Smith, D. M. Golden, M. Frenklach, N. W. Moriarty, B. Eiteneer, M. Goldenberg, C. T. Bowman, R. K. Hanson, S. Song, W. C. Gardiner, Jr., V. V. Lissianski, Z. Qin, *Gri-mech 3.0* (1999); [http://www.me.berkeley.edu/gri\\_mech/](http://www.me.berkeley.edu/gri_mech/).
29. N. S. Titova, P. S. Kuleshov, A. M. Starik, *Combust. Explos. Shock Waves* **47** (2011) 249.
30. D. O. Lignell, G. C. Fredline, A. D. Lewis, *Proc. Combust. Inst.* **35** (2015) 1199.
31. C. Chi, G. Janiga, A. Abdelsamie, K. Zähringer, T. Turányi, D. Thévenin, *Flow Turbul. Combust.* **98** (2017) 1117.